

DMS-Net: Dual-Modal Multi-Scale Siamese Network for Binocular Fundus Image Classification

Guohao Huo^{1†}, Zibo Lin^{1†}, Zitong Wang^{1†}, Ruiting Dai¹, Hao Tang^{2*}

¹University of Electronic Science and Technology of China

²Peking University

gh.huo513@gmail.com, linzibo999@gmail.com, elthinshorde6y6@gmail.com,
rtdai@uestc.edu.cn, hao.tang@vision.ee.ethz.ch

Abstract

Ophthalmic diseases pose a significant global health burden. However, traditional diagnostic methods and existing monocular image-based deep learning approaches often overlook the pathological correlations between the two eyes. In practical medical robotic diagnostic scenarios, paired retinal images (binocular fundus images) are frequently required as diagnostic evidence. To address this, we propose DMS-Net—a dual-modal multi-scale siamese network for binocular retinal image classification. The framework employs a weight-sharing siamese ResNet-152 architecture to concurrently extract deep semantic features from bilateral fundus images. To tackle challenges like indistinct lesion boundaries and diffuse pathological distributions, we introduce the OmniPool Spatial Integrator Module (OSIM), which achieves multi-resolution feature aggregation through multi-scale adaptive pooling and spatial attention mechanisms. Furthermore, the Calibrated Analogous Semantic Fusion Module (CASFM) leverages spatial-semantic recalibration and bidirectional attention mechanisms to enhance cross-modal interaction, aggregating modality-agnostic representations of fundus structures. To fully exploit the differential semantic information of lesions present in bilateral fundus features, we introduce the Cross-Modal Contrastive Alignment Module (CCAM). Additionally, to enhance the aggregation of lesion-correlated semantic information, we introduce the Cross-Modal Integrative Alignment Module (CIAM). Evaluation on the ODIR-5K dataset demonstrates that DMS-Net achieves state-of-the-art performance with an accuracy of 82.9%, recall of 84.5%, and a Cohen’s kappa coefficient of 83.2%, showcasing robust capacity in detecting symmetrical pathologies and improving clinical decision-making for ocular diseases. Code and the processed dataset will be released subsequently.

Introduction

Ophthalmic diseases have emerged as the third leading global cause of vision loss, following cardiovascular diseases and cancer. According to statistics from the World Health Organization (WHO) (World Health Organization 2019), approximately 2.2 billion people worldwide are affected by various eye conditions. Driven by population aging and the surge

in metabolic disorders (Yau et al. 2012), the prevalence of common ocular diseases such as diabetic retinopathy, glaucoma, and cataracts continues to rise. However, the uneven distribution of medical resources and the inefficiency of traditional manual diagnostics heavily reliant on clinical expertise, prevent many patients from accessing timely professional diagnosis and treatment. To address this challenge, computer vision-based ophthalmic medical robots, particularly disease diagnostic robots, are demonstrating significant potential. These systems can rapidly and automatically analyze patients’ ocular images (e.g., fundus photographs, Optical Coherence Tomography (OCT) scans), assisting clinicians in identifying signs of pathology. This technology holds promise for enhancing diagnostic efficiency and accessibility, thereby alleviating shortages in healthcare resources (Abràmoff et al. 2018).

Recent breakthroughs in computer vision technology have revolutionized ophthalmic diagnostics through deep learning-based image classification methods. Convolutional Neural Networks (CNNs), such as ResNet and EfficientNet, can automatically extract pathological features—like microaneurysms and hemorrhagic lesions—from fundus images via end-to-end learning (Ting et al. 2017). The convolution-free Vision Transformer (ViT) architecture (Xirong 2021a) leverages self-attention mechanisms to further enhance the recognition accuracy of complex pathologies, such as macular degeneration and choroidal neovascularization. Crucially, despite significant progress in monocular fundus image classification (e.g., the EfficientNet V4 model achieving 98.7% accuracy in OCT image classification (Xirong 2021b)), clinical evidence reveals that patients with unilateral ocular pathology are at substantially increased risk of developing pathological changes in the contralateral eye within subsequent years, due to shared risk factors (including genetic predisposition and oxidative stress) (Flaxman et al. 2017). Consequently, fully exploiting the underlying correlative and differential patterns in lesion spatial distribution, morphological evolution, and pathological severity between both eyes is critical for enhancing models’ capabilities in precise differential diagnosis and staging of specific diseases.

To address the aforementioned challenges, we propose DMS-Net, a framework for binocular retinal image (binocular fundus image) classification. DMS-Net integrates a siamese network architecture with fundus image analysis techniques.

It employs a weight-sharing Siamese ResNet-152 backbone to concurrently extract comprehensive deep semantic features from dual-channel (left and right eye) ocular images. Simultaneously, to tackle technical challenges in fundus pathological imaging, such as indistinct lesion boundaries, diffuse pathological distributions, and significant morphological variations, we developed the OmniPool Spatial Integrator Module (OSIM). OSIM achieves multi-resolution feature fusion through multi-scale adaptive pooling and spatial attention mechanisms.

Furthermore, we designed the Calibrated Analogous Semantic Fusion Module (CASFM) to enhance cross-modal (inter-channel) spatial-semantic interaction. CASFM utilizes spatial attention and an interactive attention-based feature recalibration mechanism to bridge semantic gaps between modalities and aggregate modality-agnostic representations of fundus structures.

Crucially, pathological manifestations in the two eyes often exhibit asymmetry (e.g., prominent hemorrhagic or exudative lesion features in one eye, with minimal or absent manifestations in the contralateral eye). This inherent disparity itself is vital for disease diagnosis. Thus, we innovatively introduce the Cross-modal Contrastive Alignment Module (CCAM) to identify and effectively leverage the differential semantic characteristics of lesions present in the left and right fundus images. Concurrently, considering the potential existence of correlative information for symmetrical pathologies between different lesions across both eyes, we propose the Cross-modal Integrative Alignment Module (CIAM) to strengthen the deep aggregation capability of lesion-correlated information extracted from the dual channels.

In summary, our contributions are as follows: (1) We proposed DMS-Net, a novel framework specifically designed for binocular retinal image classification, employing a weight-sharing Siamese ResNet-152 backbone to extract deep semantic features from both eyes simultaneously. (2) Developed the OmniPool Spatial Integrator Module (OSIM), which achieves effective multi-resolution feature fusion through multi-scale adaptive pooling and spatial attention mechanisms. (3) Designed the Calibrated Analogous Semantic Fusion Module (CASFM), which employs spatial attention and an interactive attention-based feature recalibration mechanism to bridge modality-specific semantic gaps and aggregate modality-agnostic representations of fundus structures. (4) Innovatively introduced the Cross-modal Contrastive Alignment Module (CCAM) to identify and leverage differential lesion semantics between left and right eyes. And proposed the Cross-modal Integrative Alignment Module (CIAM) to enhance the aggregation capability for lesion-correlated information across both eyes. (5) Demonstrated superior performance through extensive experiments on the ODIR-5K dataset, achieving an accuracy of 82.9%, a recall of 84.5%, and Cohen's kappa coefficient of 83.2% for binocular fundus image classification.

Related Work

Development of Fundus Image Classification Tasks

In recent years, there has been a marked upward trend in the global incidence of ophthalmic diseases. To enhance di-

agnostic efficiency and alleviate pressures stemming from healthcare resource shortages, intelligent computer-aided diagnosis (CAD) systems based on retinal images (fundus images)—serving as the core component of ophthalmic diagnostic robotics—demonstrate substantial value in reducing diagnostic time for medical professionals and improving the efficiency of clinical decision-making. In the early research stage, (García-Florian et al. 2019) proposed a Support Vector Machine (SVM) combined with mathematical morphology and digital image processing techniques, achieving a high accuracy in the task of detecting macular lesions. Subsequently, the study (S., Gopi, and Palanisamy 2020) inputs the features extracted by the Convolutional Neural Network (CNN) into various machine learning classifiers such as SVM, Random Forest, Multi-Layer Perceptron (MLP), and J48, also achieving excellent results with a relatively small number of parameters. However, as the feature dimensions become more complex and the data scale expands, traditional methods gradually show limitations in the generalization ability of the model. For example, the feature extraction method relying on the maximum principal curvature algorithm and the eigenvalues of the Hessian matrix in (Das et al. 2021) is too simple and fails to take into account the complex information integration requirements of multiple scales and cross-modalities. With the breakthroughs in deep learning, Convolutional Neural Networks (CNNs) have become the mainstream method for the classification of diseases in fundus images. (Wang et al. 2020) developed a multi-classification model using EfficientNet, which performed well on a small-scale dataset. However, excessive focus on local lesion features led to the neglect of global context relationships. This limitation also exists in the SqueezeNet model proposed in (Thanki 2023). Although its pure CNN architecture can obtain multi-scale information through the squeeze convolutional layer, it is still difficult to fully mine the detailed features of the image, resulting in insufficient utilization of information. On this basis, (Yang, Chen, and Xu 2021) innovatively proposed the TransEye model, combining the local perception advantages of CNNs with the global attention mechanism of the Transformer. This hybrid architecture echoes the MIL-VT framework introduced in (Yu et al. 2021). The latter confirms the feasibility of global modeling through Transformer pre-training, but still fails to solve key problems such as lesion boundaries. At the same time, clinical studies have shown that patients with unilateral lesions have a significantly increased risk of developing symmetric lesions in the contralateral eye (Flaxman et al. 2017). Although existing technologies have made progress in monocular classification, for example, (S., Gopi, and Palanisamy 2020) achieves feature fusion through the bottleneck layer module, there are still deficiencies in the collaborative analysis of both eyes and the prediction of disease progression. These studies have promoted the development of the field from different perspectives, such as innovative feature extraction algorithms, integration of multiple classifiers, and architectural fusion. Existing research has propelled advancements in this field from various dimensions, including the design of innovative feature extraction algorithms, the development of multi-classifier integration strategies, and the optimization of model architecture fusion.

Nevertheless, these studies also reveal that current methodologies exhibit limitations in cross-regional feature modeling capability and effective integration of multi-modal information. This delineates critical research priorities for future work.

Siamese Network-Based Classification of Binocular Fundus Images

Since the Siamese network model was first applied to handwritten signature verification by (Bromley et al. 1993), this architecture has demonstrated significant advantages in image matching and classification tasks. Its weight-sharing property is highly sensitive to changes in similarity features, and it is particularly adept at homologous object recognition tasks. In the context of few-shot learning, (Wang and Wang 2019) introduced the siamese network into plant leaf classification. By constructing a metric space through a parallel dual-channel convolutional network, they significantly improved the classification accuracy. This property has also been verified in the field of medical imaging: (Lin et al. 2022) compared the performance of traditional single-image input and the siamese network in glaucoma recognition, confirming the good performance and generalization of the latter, and also pointing out that the model can be further optimized through attention mechanisms. The applications in the field of medical imaging are continuously evolving and deepening. (Zeng et al. 2019) verified the effectiveness of the siamese network in capturing binocular collaborative features by comparing monocular and binocular fundus image models. (Nirthika, Manivannan, and Ramanan 2022) innovatively adopted bilinear pooling technology in the grading of diabetic retinopathy, successfully capturing the non-linear correlations between the binocular lesion areas. Meanwhile, the study (Akella and Kumar 2024) shows that the method using the monocular YOLO V3 algorithm not only ignores the lesion associations between binocular images but also struggles to solve the problems of blurred boundaries and scattered features, highlighting the unique value of the siamese architecture. In terms of feature optimization and architectural innovation, (Inan 2024) integrated multimodal processing methods such as edge detection and color separation to achieve a fine-grained representation of fundus image features. However, the study (Chen, Zhao, and Zhou 2024) points out that existing methods, such as simply concatenating features, fail to fully explore the potential relationships between features and have extremely low utilization of multi-scale information. The dual-stream interaction framework designed by (Yang, Chen, and Xu 2021) enhances the dynamic association between local and global features through an attention mechanism, which echoes the research (Tan, Dong, and Li 2023) that employs a siamese network and an attention mechanism. However, the latter only performs channel concatenation in the feature concatenation step, resulting in insufficient utilization of spatial structure information. It is worth noting that although the adaptive pooling and attention mechanism proposed in (Tariq, Palade, and Ma 2024) achieves multi-resolution feature aggregation, there is still a problem of semantic information loss in the processing of complex images. Although current research has made progress in modeling paired modal differential features,

as revealed by studies such as (Chen, Zhao, and Zhou 2024), it still faces problems such as incomplete feature fusion and insufficient cross-modal information integration. This study aims to break through the representational dimensional limitations of existing Siamese networks by incorporating a morphological-semantic spatial feature learning mechanism, providing a new technical approach to address the above-mentioned issues.

Classification of Binocular Fundus Images Combined with Ophthalmic Robotics

Fundus image recognition technology is closely related to the development of ophthalmic robots and telemedicine. (Madanan et al. 2025) reviews the role of artificial intelligence and image recognition in surgical area identification and real-time feedback adjustment, providing support for improving surgical accuracy and the feasibility of remote surgery. In 2021, (Khan, Kallogjeri, and Piccirillo 2021) first applied deep learning to self-calibrated OCT system images, demonstrating the potential of integrating AI with robotic ocular imaging in automated eye disease screening. However, this technology still requires implementation by professional physicians and has higher requirements for autonomy. With the improvement of robot precision, (Li et al. 2022b) studied an automatic drug injection device for robot-assisted retinal vein injection surgery, verifying its reliability. In terms of telemedicine, (Thainimit et al. 2022) evaluated the efficiency and usability of robotic process automation and machine learning in remote ophthalmic screening, showing good results in saving time, improving satisfaction, and reducing the workload of medical staff. Afterwards, telemedicine still requires intelligence and ease of use to get rid of dependence on high-level physicians. (Foust et al. 2025) reviews new directions in diagnostic robots. The robot studied therein can assist non-ophthalmologists in diagnosing fundus abnormalities and improve the efficiency of pathological recognition by combining deep learning models. The ophthalmic disease diagnostic robot studied in (Li et al. 2024) can automatically collect ocular surface and fundus images without the operation of ophthalmologists, solving the problem of a shortage of professionals in remote areas and lowering the threshold for telemedicine implementation. Ophthalmic diagnosis has high requirements for image clarity, and numerous studies have promoted the progress of image capture. (Pan et al. 2024) reduces motion artifacts in captured images and improves the accuracy of model recognition. (Draeos et al. 2023) breaks through the limitations of traditional photography technology on patient posture and head orientation, improving adaptability in different scenarios. (Zhou et al. 2025) realizes functions such as automatic obstacle avoidance and dynamic tracking of mobile robots, strengthens scene adaptability and automation capabilities, and reduces requirements for operators.

The Proposed Method

We propose DMS-Net, a Siamese network-based framework for binocular retinal image (binocular fundus image) classification. As shown in Figure 1, our fundus disease diagnosis robot incorporating DMS-Net demonstrates its workflow.

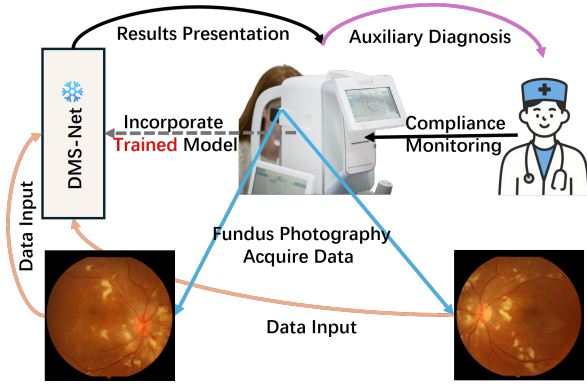


Figure 1: Workflow Diagram of a Fundus Imaging Disease Diagnosis Robot with Integrated DMS-Net. Clinicians continuously monitor the use of the fundus imaging diagnosis robot. The device scans the patient’s retina to acquire fundus images, which are then processed by its integrated, trained DMS-Net model. Disease classification results are displayed on-screen to assist in physician diagnosis.

As illustrated in Figure 2, the model employs dual weight-sharing ResNet-152 branches to concurrently extract deep semantic features from dual-channel (left-right) ocular images. To effectively address the challenges of indistinct lesion boundaries and morphological heterogeneity, our method innovatively incorporates the OmniPool Spatial Integrator Module (OSIM). OSIM integrates multi-scale adaptive average pooling (Adaptive Average Pooling), global max pooling (Global Max Pooling), and a spatial attention mechanism (Spatial Attention Mechanism).

Furthermore, we designed the Calibrated Analogous Semantic Fusion Module (CASFM), which leverages spatial attention, bidirectional cross-attention mechanisms, and parametrically adaptive residual connections to facilitate cross-modal (inter-channel) spatial-semantic interaction.

To comprehensively identify and effectively leverage the differential semantic information of lesion features present in the left and right retinal images (fundus images), we introduce the Cross-modal Contrastive Alignment Module (CCAM). Concurrently, considering the existence of correlative information for symmetrical pathologies across different lesions in both eyes, we designed the Cross-modal Integrative Alignment Module (CIAM) to enhance the deep aggregation of lesion-correlated information extracted from the dual channels, thereby generating more discriminative representations.

Siamese Network Feature Extraction

In this study, we constructed a binocular retinal image (fundus image) feature extraction backbone network based on a pre-trained ResNet-152 architecture. Implementing a weight-sharing strategy to achieve synchronized parameter updates, the network enables parallel extraction of deep semantic features from paired left-right retinal (fundus) images. This design effectively captures morphological feature correlations in lesion regions across both fundus images, alongside their high-level semantic representations.

OmniPool Spatial Integrator Module (OSIM)

To address the technical challenges of boundary ambiguity, scattered lesion distribution, and significant morphological variations in retinal lesion images, this study proposes an innovative OmniPool Spatial Integrator Module (OSIM). The module architecture diagram is shown in Figure 2. The module builds upon high-level semantic features extracted by the ResNet152 network and employs a multi-scale pooling-based feature enhancement strategy: Adaptive Average Pooling with a scale parameter of 2 captures medium-grained semantic representations, while adaptive pooling operations with a scale parameter of 4 extract coarse-grained semantic features:

$$\text{SPP}_{2 \times 2}(x) = \text{interp} \left(\text{avgpool}_{(2,2)}(x), \text{size} = H \times W \right) \quad (1)$$

$$\text{SPP}_{4 \times 4}(x) = \text{interp} \left(\text{avgpool}_{(4,4)}(x), \text{size} = H \times W \right) \quad (2)$$

In the formula, $x \in \mathbb{R}^{H \times W \times C}$ denotes the high-level semantic features extracted by the ResNet152 network. Here, interp represents bilinear interpolation mode = bilinear to restore the feature map to its original dimensions $H \times W$. This is followed by the integration of Global Max Pooling to enhance feature responses in salient lesion regions:

$$\text{GMP}(x) = \text{maxpool}_{(1,1)}(x) \odot \mathbf{1} \quad (3)$$

To capture global contextual semantic information, we also introduce Global Average Pooling:

$$\text{GAP}(x) = \text{avgpool}_{(1,1)}(x) \odot \mathbf{1} \quad (4)$$

In the formula, \odot denotes element-wise multiplication, where the tensor $\mathbf{1}$ (all-ones) is broadcast to match the original dimensions $H \times W$. To alleviate the potential loss of subtle lesion features caused by pooling operations, a supplementary mechanism is specifically designed to retain the original high-level semantic features.

$$F_{\text{input}} = \text{Concat}(x, \text{GMP}(x), \text{GAP}(x), \text{SPP}_{(2 \times 2)}(x), \text{SPP}_{(4 \times 4)}(x), \text{dim} = 1) \quad (5)$$

Specifically, the Concat operation is employed to fuse semantic features of five different scales along the channel dimension, resulting in a combined feature map $X \in \mathbb{R}^{H \times W \times 5C}$. This fused representation is then fed into a channel compression mechanism for adaptive channel-wise fusion.

$$F_{\text{ccp}} = \text{ReLU}(\text{BatchNorm}(\text{Conv2d}_{(1 \times 1)}(F_{\text{input}}))) \quad (6)$$

The five types of multi-scale features (including the original high-level semantic features, two-scale pooling features, and two global pooling features) are adaptively fused through 2D convolution operations to obtain $F_{\text{ccp}} \in \mathbb{R}^{H \times W \times (C/2)}$. Finally, a spatial attention mechanism is applied to strengthen the feature responses in lesion regions.

$$F_{\text{out}} = F_{\text{ccp}} \odot \sigma(W_s * F_{\text{ccp}} + b_s) \quad (7)$$

In the formula, σ denotes the Sigmoid activation function, and $F_{\text{out}} \in \mathbb{R}^{H \times W \times (C/2)}$ represents the output of the multi-scale feature extraction module integrated with a spatial attention mechanism. This integration aims to achieve focused enhancement of critical pathological features.

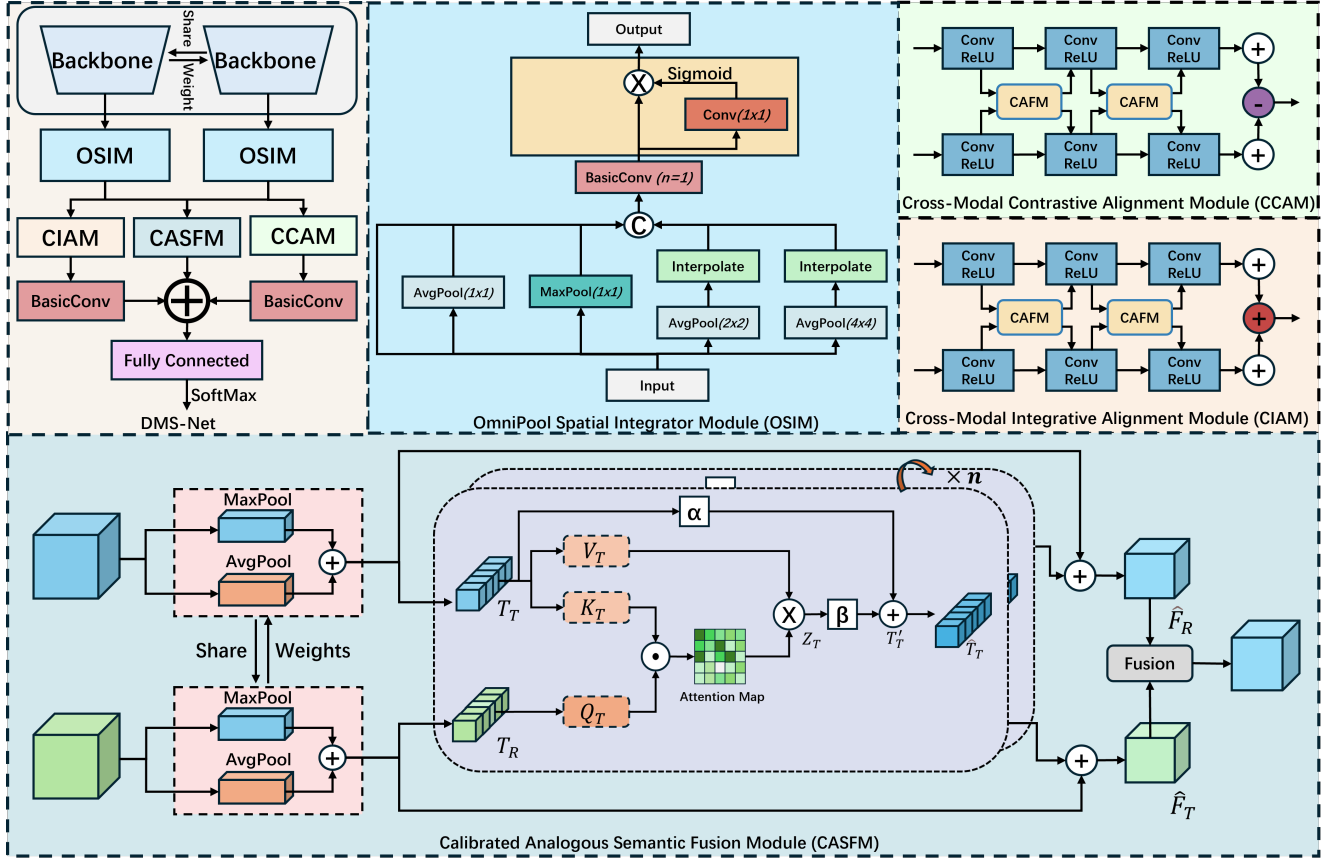


Figure 2: The architecture of DMS-Net.

Calibrated Analogous Semantic Fusion Module (CASFM)

To enhance the performance of Siamese networks in spatial-semantic representation of lesion localization and tissue structure correlation, this study designs a Calibrated Analogous Semantic Fusion Module (CASFM). The architecture diagram of the CASFM is as shown in Figure 2. This module constructs a modality-agnostic semantic representation system for lesions through multi-scale cross-modal feature spatial-semantic extraction and cross-modal fusion. Specifically, the CASFM module adopts a dual-path parallel processing framework:

First, max-pooling and average-pooling operations are applied to the input binocular features to achieve spatial dimension compression.

$$F_{left/right}^{avg} = \frac{1}{k^2} \text{avgpool}(\text{Conv2d}_{(1 \times 1)}(F_{left/right}))$$

$$F_{left/right}^{max} = \frac{1}{k^2} \text{maxpool}(\text{Conv2d}_{(1 \times 1)}(F_{left/right}))$$

(8)

In the formula, k denotes the size of the pooling kernel. We set $k = 2$, and the input features $F_{right/left} \in \mathbb{R}^{H \times W \times (C/2)}$ correspond to the output F_{out} from the multi-scale feature extraction module. Multi-granularity feature fusion is implemented via learnable modality-adaptive weighting factors

$\lambda_{left/right} \in [0, 1]$, effectively preserving global contextual information and local detail features of lesions:

$$F_{left} = \lambda_{left} \cdot F_{left}^{max} + (1 - \lambda_{left}) \cdot F_{left}^{avg}$$

$$F_{right} = \lambda_{right} \cdot F_{right}^{max} + (1 - \lambda_{right}) \cdot F_{right}^{avg}$$

(9)

To mitigate interference from spatial positional deviations of binocular fundus high-level semantic features on lesion semantic alignment, modality-specific spatial embedding vectors are introduced for positional encoding compensation:

$$F'_{left/right} = \text{Flatten}(\text{Conv2d}_{(1 \times 1)}(F_{left/right}))$$

$$+ \text{Interp}(P_0, (H, W)) \cdot W_p$$

(10)

In the formula, $P_0 \in \mathbb{R}^{C_{emb} \times 1 \times 1}$ denotes the initial positional embedding parameters. A bidirectional multi-head attention mechanism establishes cross-modal feature interaction channels, achieving collaborative enhancement of lesion semantics across different subspaces:

$$Z_{right} = \text{softmax}\left(\frac{Q_{left} K_{right}^T}{\sqrt{D_K}}\right) \cdot V_{right}$$

$$Z_{left} = \text{softmax}\left(\frac{Q_{right} K_{left}^T}{\sqrt{D_K}}\right) \cdot V_{left}$$

(11)

A parameter-adaptive residual connection strategy fuses enhanced features with original features:

$$\begin{aligned} T'_{left} &= \alpha_{left} \cdot Z_{left} \cdot W^O + \beta_{left} \cdot T_{left} \\ T'_{right} &= \alpha_{right} \cdot Z_{right} \cdot W^O + \beta_{right} \cdot T_{right} \end{aligned} \quad (12)$$

In the formula, $\alpha_{left/right} \in [0, 1]$ and $\beta_{left/right} \in [0, 1]$ denote adaptive fusion parameters.

Finally, the modality-disentangled dual-branch spatial-semantic features are adaptively fused to reconstruct modality-agnostic spatial-semantic feature information:

$$F_{fuse} = \text{Conv2d}_{(1 \times 1)}(\text{Concat}(\hat{T}_{left}, \hat{T}_{right})) \quad (13)$$

Dual-Synergy Cross-Modal Fusion

To better align and fuse the semantic relationships between features of binocular retinal (fundus) images, we designed the Cross-Modal Contrastive Alignment Module (CCAM) and the Cross-Modal Integrative Alignment Module (CIAM) to operate in parallel. As shown in Figure 2, CCAM captures differential pathological features between left-right ocular images, while CIAM aggregates and enhances interocular lesion-correlated semantic features.

Cross-Modal Contrastive Alignment Module (CCAM)

In conditions like diabetic retinopathy, binocular (bilateral) ocular pathology often manifests asymmetrically (e.g., significant hemorrhage in the left eye versus mild pathology in the right eye). The CCAM leverages the Cross-Attention Fusion Module (CAFM) to compute the distributional discrepancy between cross-eye features. It then guides the dual-path densely connected convolutional network to progressively achieve pathological-asymmetry-aligned semantic representations of binocular lesions. This mechanism directs the model to concentrate on asymmetry characteristics among lesions, such as disparities in hemorrhage extent and exudate morphology.

Cross-Modal Integrative Alignment Module (CIAM)

In diseases such as glaucoma and hypertensive retinopathy, there exist symmetrically co-evolving pathological patterns (e.g., synchronous enlargement of the cup-to-disc ratio, symmetric increase in vascular stenosis severity). The CIAM leverages the Cross-Attention Fusion Module (CAFM) to mine and quantify interocular symmetrical pathological correlations, exemplified by computing spatial similarity of feature maps across key anatomical regions (e.g., optic disc localization), and achieves lesion region alignment (like optic disc co-registration). Subsequently, the module guides the dual-path densely connected convolutional network towards synergistic enhancement of binocular pathological semantic features, while employing residual connections to preserve the original feature information and mitigate critical information loss.

Dataset

ODIR-5K (KOTO 2020) is a structured medical imaging dataset dedicated to ophthalmic disease intelligent recognition. Jointly released by Peking University and institutions

including Shanghai Medical Technology in 2019, it aims to advance the application of artificial intelligence in fundus disease classification. The dataset contains anonymized clinical data from 5,000 patients, with each patient record encompassing gender, age, color fundus photographs of both eyes, and physicians' diagnostic keywords.

Data process

We employed non-uniform illumination correction preprocessing for image optimization, combined with the CutMix data augmentation algorithm to integrate local regions of homogeneous samples while preserving original class labels. This strategy effectively guides the model to focus on learning more discriminative local features, achieving diversified dataset expansion while maintaining lesion region consistency, thereby enhancing model generalization capability. Considering the class imbalance in the original dataset objectively reflects epidemiological characteristics of real-world disease distribution, a class distribution preservation strategy was implemented during data preprocessing to moderately maintain the inherent class imbalance. This approach ensures the model effectively learns clinically representative data distribution patterns. Figures 4 and 5 present our raw data and the step-by-step data processing visualization results.

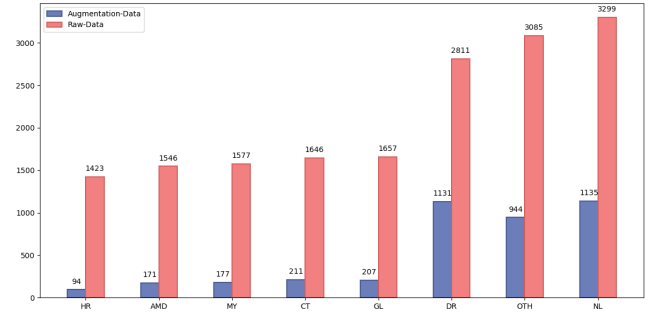


Figure 3: Comparison of raw data versus augmented data quantities. Note the significant increase in sample size after augmentation.

The figure 3 illustrates the distribution of fundus image data across various ophthalmic disease categories (including normal samples) in the original dataset and their corresponding quantities after data processing. The abbreviations on the bar chart's horizontal axis correspond to the following ophthalmic conditions: N (NL) denotes Normal, D (DR) represents Diabetic Retinopathy, G (GL) indicates Glaucoma, C (CT) corresponds to Cataract, A (AMD) signifies Age-related Macular Degeneration, H (HR) refers to Hypertensive Retinopathy, M (MY) stands for Myopia, and O (OTH) designates Other Disease. This standardized labeling system uses initial letter abbreviations to maintain clarity in visualizing epidemiological data distributions across disease categories.

Ablation Study

We utilize Accuracy (Acc) to quantify the overall correctness of model predictions, Precision to evaluate the reliability of positive-class predictions, and Recall to assess the model's

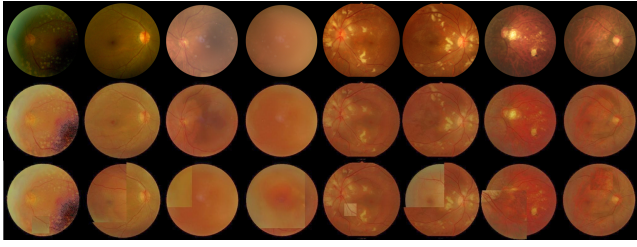


Figure 4: The first row displays four pairs of original fundus imaging data, sequentially presenting cases of diabetic retinopathy, cataract, hypertensive retinopathy, and high myopia. The second row shows enhanced images after non-uniform illumination correction processing. The third row demonstrates newly synthesized data generated by applying CutMix augmentation on the illumination-corrected images.

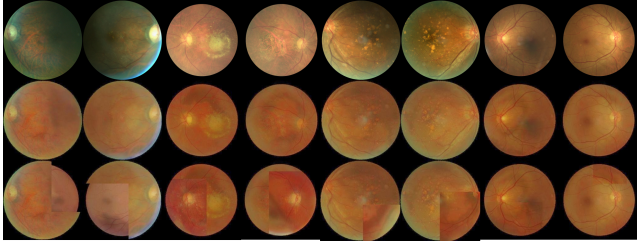


Figure 5: The first row displays four pairs of original fundus imaging data, from left to right, respectively representing other ocular pathologies, glaucoma, macular degeneration, and normal retinal structures. The second row demonstrates enhanced images after non-uniform illumination correction processing. The third row exhibits newly synthesized data generated by implementing CutMix augmentation on the illumination-corrected images.

ability to capture true positive samples. The Kappa Coefficient measures the statistical divergence between classification results and random predictions, while the F1 Score balances Precision and Recall through a harmonic mean. AUC (Area Under the ROC Curve) further characterizes the model’s capability to distinguish between positive and negative classes. By integrating these multidimensional metrics, we comprehensively evaluate the model’s performance.

We conducted experiments to explore the following two aspects: (1) the model performance using different backbones as feature extractors, and the experimental results are shown in Table 1; (2) the effectiveness of each component of the model, and the experimental results are shown in Table 2.

Model Performance with Different Backbones

The ablation study comparing the impact of different backbone networks on model performance reveals that ResNet-152 consistently achieves the highest performance across all metrics (as shown in Table 1), including accuracy, precision, recall, Kappa coefficient, F1-score, and area under the curve (AUC), with an accuracy of 0.829 and an AUC of 0.973, indicating its superiority in feature extraction and classification stability; in contrast, the Vision Transformer (ViT) demonstrates relatively weaker performance with lower

metrics (e.g., accuracy at 0.804), highlighting its limitations for the task, while the ResNet series exhibits progressive improvement in performance with increasing depth (e.g., from ResNet-50 to ResNet-152), underscoring the positive effect of model complexity on precision.

Table 1: Model Performance with Different Backbones

Backbone	Acc	Precision	Recall	Kappa	F1	AUC
ViT	0.804	0.826	0.826	0.797	0.825	0.949
ResNeXt	0.792	0.827	0.806	0.784	0.812	0.962
ResNet-50	0.817	0.854	0.827	0.812	0.837	0.962
ResNet-101	0.819	0.860	0.825	0.814	0.839	0.965
ResNet-152	0.829	0.869	0.845	0.832	0.856	0.973

Investigation into the Effectiveness of Model Components

As delineated in Table 2, quantitative ablation studies rigorously validate the contribution of each module. Removing the CASFM causes the most severe degradation: Kappa coefficient declines by 2.5% (0.832 to 0.807), accuracy drops 1.7% (0.829 to 0.812), with an equivalent 1.7% recall reduction (0.845 to 0.828). The dual-synergy modules also demonstrate critical roles: eliminating the CCAM reduces accuracy by 1.0% (0.829 to 0.819), whereas removing the CIAM leads to a 1.3% accuracy decrease (0.829 to 0.816). The integrity of the OSIM is vital for model stability, as ablation of its left sub-module decreases Kappa by 1.3% (0.832 to 0.819), and right sub-module removal results in 2.0% Kappa reduction (0.832 to 0.812). The full model (ALL) achieves optimal performance across all metrics, with its 0.973 AUC and 0.856 F1-score substantially surpassing any ablated configuration.

Table 2: Investigation into the Effectiveness of Model Components

Configuration	Acc	Precision	Recall	Kappa	F1	AUC
w/o CAFM	0.819	0.854	0.829	0.815	0.840	0.967
w/o CIAM	0.816	0.856	0.829	0.815	0.841	0.962
w/o CCAM	0.819	0.859	0.836	0.822	0.848	0.963
w/o CASFM	0.812	0.844	0.828	0.807	0.834	0.960
w/o OSIM(Left)	0.816	0.853	0.837	0.819	0.845	0.961
w/o OSIM(Right)	0.818	0.850	0.830	0.812	0.838	0.963
w/o OSIM(ALL)	0.822	0.857	0.835	0.817	0.843	0.965
ALL	0.829	0.869	0.845	0.832	0.856	0.973

Model Performance with Different Feature Extraction Module

We investigated the impact of different plug-and-play multi-scale modules on model performance, as shown in Table 3, where our OSIM module was replaced with ASPP (Chen et al. 2018), SPPF (Khanam and Hussain 2024), SPP (He et al. 2015), RFB (Liu, Huang, and Wang 2018), and SimSPPF (Li et al. 2022a) variants. Ablation experiments confirmed that the proposed OSIM module achieves superior performance compared to these alternatives.

Table 3: Model Performance with Different Feature Extraction Module.

Backbone	Acc	Precision	Recall	Kappa	F1	AUC
ASPP	0.776	0.816	0.793	0.769	0.800	0.958
SPPF	0.774	0.828	0.799	0.778	0.807	0.964
SPP	0.805	0.836	0.821	0.800	0.827	0.965
simSPPF	0.792	0.827	0.807	0.784	0.812	0.961
RFB	<u>0.824</u>	<u>0.867</u>	<u>0.832</u>	<u>0.828</u>	<u>0.852</u>	<u>0.971</u>
OSIM (Ours)	0.829	0.869	0.845	0.832	0.856	0.973

Conclusion

This study proposes DMS-Net for binocular retinal image classification – a dual-modal multi-scale siamese network framework. By integrating a weight-sharing Siamese ResNet-152 backbone, the multi-scale context aggregation module (OSIM), and the Calibrated Analogous Semantic Fusion Module (CASFM), the framework effectively addresses core challenges in binocular fundus image analysis: indistinct lesion boundaries, diffuse pathological distributions, and cross-modal (dual-channel) information interaction. OSIM achieves robust extraction of multi-resolution pathological features through its hierarchical multi-scale pooling structure (improving Kappa coefficient by 0.8% over the best baseline). CASFM leverages spatial attention and feature recalibration mechanisms to capture and enhance discriminative, modality-agnostic pathological semantic representations. Crucially, the innovatively designed Cross-modal Contrastive Alignment Module (CCAM) and Cross-modal Integrative Alignment Module (CIAM) achieve, for the first time, a synergistic modeling mechanism for asymmetric lesion manifestations (e.g., unilateral hemorrhage) and symmetrically evolving pathological patterns (e.g., bilateral synchronous changes in cup-to-disc ratio). This study contributes to enhancing the diagnostic precision and reliability of existing ophthalmic robots when processing complex fundus images characterized by asymmetric lesions, indistinct boundaries, and other complexities. Evaluated on the ODIR-5K dataset, DMS-Net sets a new state-of-the-art performance with an accuracy of 82.9%, a recall of 84.5%, and a Cohen’s Kappa coefficient of 83.2%.

References

- Abràmoff, M. D.; Lavin, P. T.; Birch, M.; Shah, N.; and Folk, J. C. 2018. Pivotal trial of an autonomous AI-based diagnostic system for detection of diabetic retinopathy in primary care offices. *NPJ digital medicine*, 1(1): 39.
- Akella, P.; and Kumar, R. 2024. An advanced deep learning method to detect and classify diabetic retinopathy based on color fundus images. *Graefes Arch Clin Exp Ophthalmol*, 262: 231 – 247.
- Bromley, J.; Guyon, I.; LeCun, Y.; Säckinger, E.; and Shah, R. 1993. Signature Verification Using a Siamese Time Delay Neural Network. In Cowan, J. D.; Tesauro, G.; and Alspector, J., eds., *Advances in Neural Information Processing Systems 6, [7th NIPS Conference, Denver, Colorado, USA, 1993]*, 737–744. Morgan Kaufmann.
- Chen, F.; Zhao, W.; and Zhou, X. 2024. Cross-Image siamese graph convolutional network for Fine-Grained image retrieval in diabetic retinopathy. *Biomedical Signal Processing and Control*, 92: 106045.
- Chen, L.; Papandreou, G.; Kokkinos, I.; Murphy, K.; and Yuille, A. L. 2018. DeepLab: Semantic Image Segmentation with Deep Convolutional Nets, Atrous Convolution, and Fully Connected CRFs. *IEEE Trans. Pattern Anal. Mach. Intell.*, 40(4): 834–848.
- Das, S.; Kharbanda, K.; M, S.; Raman, R.; and D, E. D. 2021. Deep learning architecture based on segmented fundus image features for classification of diabetic retinopathy. *Biomedical Signal Processing and Control*, 68: 102600.
- Draeos, M.; Ortiz, P.; Narawane, A.; McNabb, R. P.; Kuo, A. N.; and Izatt, J. A. 2023. Robotic Optical Coherence Tomography of Human Subjects with Posture-Invariant Head and Eye Alignment in Six Degrees of Freedom. In *2023 International Symposium on Medical Robotics (ISMR)*, 1–7.
- Flaxman, S. R.; Bourne, R. R.; Resnikoff, S.; Ackland, P.; Braithwaite, T.; Cicinelli, M. V.; Das, A.; Jonas, J. B.; Keeffe, J.; Kempen, J. H.; et al. 2017. Global causes of blindness and distance vision impairment 1990–2020: a systematic review and meta-analysis. *The Lancet Global Health*, 5(12): e1221–e1234.
- Foust, J.; McCloud, M.; Narawane, A.; Trout, R. M.; Chen, X.; Dhalla, A.-H.; Li, J. D.; Viehland, C.; Draeos, M.; Vajzovic, L.; McNabb, R. P.; Kuo, A. N.; and Toth, C. A. 2025. New Directions for Ophthalmic OCT – Handhelds, Surgery, and Robotics. *Translational Vision Science & Technology*, 14(1): 14–14.
- García-Florian, A.; Ferreira-Santiago, Á.; Nieto, O. C.; and Yáñez-Márquez, C. 2019. A machine learning approach to medical image classification: Detecting age-related macular degeneration in fundus images. *Comput. Electr. Eng.*, 75: 218–229.
- He, K.; Zhang, X.; Ren, S.; and Sun, J. 2015. Spatial Pyramid Pooling in Deep Convolutional Networks for Visual Recognition. *IEEE Trans. Pattern Anal. Mach. Intell.*, 37(9): 1904–1916.
- Inan, Y. S. 2024. Adaptive Multiscale Retinal Diagnosis: A Hybrid Trio-Model Approach for Comprehensive Fundus Multi-Disease Detection Leveraging Transfer Learning and Siamese Networks. *CoRR*, abs/2405.18449.
- Khan, A. M.; Kallogjeri, D.; and Piccirillo, J. F. 2021. 51152 Efficacy of Bimodal Visual-Olfactory Training in Patients with COVID-19 resultant Hyposmia or Anosmia Using Patient-Preferred Scents (VOLT Trial - Visual-OLfactory Training). *Journal of Clinical and Translational Science*, 5(s1): 122–122.
- Khanam, R.; and Hussain, M. 2024. What is YOLOv5: A deep look into the internal features of the popular object detector. *arXiv preprint arXiv:2407.20892*.
- KOTO. 2020. ODIR-5K. <https://www.heywhale.com/mw/dataset/5e95e3ede7ec38002d0351f6>.
- Li, C.; Li, L.; Jiang, H.; Weng, K.; Geng, Y.; Li, L.; Ke, Z.; Li, Q.; Cheng, M.; Nie, W.; et al. 2022a. YOLOv6: A single-stage object detection framework for industrial applications. *arXiv preprint arXiv:2209.02976*.
- Li, Q.; Tan, J.; Xie, H.; Zhang, X.; Dai, Q.; Li, Z.; Yan, L. L.; and Chen, W. 2024. Evaluating the accuracy of the Ophthalmologist Robot for multiple blindness-causing eye diseases: a multicentre, prospective study protocol. *BMJ Open*, 14(3).
- Li, Z.; Fu, P.; Wei, B.-T.; Wang, J.; Li, A.-L.; Li, M.-J.; and Bian, G.-B. 2022b. An automatic drug injection device with spatial micro-force perception guided by an microscopic image for robot-assisted ophthalmic surgery. *Frontiers in Robotics and AI*, Volume 9 - 2022.
- Lin, M.; Liu, L.; Gordon, M.; Kass, M.; Wang, F.; Van Tassel, S. H.; and Peng, Y. 2022. Primary Open-Angle Glaucoma Diagnosis from Optic Disc Photographs Using a Siamese Network. *Ophthalmology Science*, 2(4): 100209.
- Liu, S.; Huang, D.; and Wang, Y. 2018. Receptive Field Block Net for Accurate and Fast Object Detection. In Ferrari, V.; Hebert, M.; Sminchisescu, C.; and Weiss, Y., eds., *ECCV 2018*, volume 11215 of *Lecture Notes in Computer Science*, 404–419. Springer.
- Madanan, M.; Gunasekaran, S. S.; Mahmoud, M. A.; Dhillon, J. S.; Mostafa, S.; and Nidzam, N. N. S. 2025. *Artificial Intelligence Methods and Image Recognition Techniques in Ophthalmic Robotic Surgery: A Review*, 345–364. Cham: Springer Nature Switzerland. ISBN 978-3-031-75091-5.
- Nirithika, R.; Manivannan, S.; and Ramanan, A. 2022. Siamese network based fine grained classification for Diabetic Retinopathy grading. *Biomedical Signal Processing and Control*, 78: 103874.
- Pan, H.; Lim, C. W.; King, K.; Guan, R.; and Draeos, M. 2024. Active Motion Cancellation for Robotic Optical Coherence Tomography of Moving Eyes: A Nystagmus Phantom Study. In *2024 International Symposium on Medical Robotics (ISMR)*, 1–7.
- S., G.; Gopi, V. P.; and Palanisamy, P. 2020. A lightweight CNN for Diabetic Retinopathy classification from fundus images. *Biomedical Signal Processing and Control*, 62: 102115.
- Tan, J.; Dong, Y.; and Li, J. 2023. Automated fundus ultrasound image classification based on siamese convolutional neural networks with multi-attention. *BMC Med Imaging*, 23(89).

- Tariq, M.; Palade, V.; and Ma, Y. 2024. Effective Diabetic Retinopathy Classification With Siamese Neural Network: A Strategy for Small Dataset Challenges. *IEEE Access*, 12: 182814–182827.
- Thainimit, S.; Chaipayom, P.; Sa-arnwong, N.; Gansawat, D.; Petchyim, S.; and Pongrujikorn, S. 2022. Robotic process automation support in telemedicine: Glaucoma screening usage case. *Informatics in Medicine Unlocked*, 31: 101001.
- Thanki, R. 2023. A deep neural network and machine learning approach for retinal fundus image classification. *Health-care Analytics*, 3: 100140.
- Ting, D. S. W.; Cheung, C. Y.-L.; Lim, G.; Tan, G. S. W.; Quang, N. D.; Gan, A.; Hamzah, H.; Garcia-Franco, R.; San Yeo, I. Y.; Lee, S. Y.; et al. 2017. Development and validation of a deep learning system for diabetic retinopathy and related eye diseases using retinal images from multiethnic populations with diabetes. *Jama*, 318(22): 2211–2223.
- Wang, B.; and Wang, D. 2019. Plant Leaves Classification: A Few-Shot Learning Method Based on Siamese Network. *IEEE Access*, 7: 151754–151763.
- Wang, J.; Yang, L.; Huo, Z.; He, W.; and Luo, J. 2020. Multi-Label Classification of Fundus Images With EfficientNet. *IEEE Access*, 8: 212499–212508.
- World Health Organization. 2019. *World report on vision*. Geneva.
- Xirong, L. 2021a. Multi-modal deep learning and its applications in ophthalmic artificial intelligence. *Medical Journal of Peking Union Medical College Hospital*, 12(5): 602–607.
- Xirong, L. 2021b. Multi-modal deep learning and its applications in ophthalmic artificial intelligence. *Medical Journal of Peking Union Medical College Hospital*, 12(5): 602–607.
- Yang, H.; Chen, J.; and Xu, M. 2021. Fundus Disease Image Classification based on Improved Transformer. In *2021 International Conference on Neuromorphic Computing (ICNC)*, 207–214.
- Yau, J. W. J.; Rogers, S. L.; Kawasaki, R.; Lamoureux, E. L.; Kowalski, J. W.; Bek, T.; Chen, S. J.; Dekker, J. M.; Fletcher, A.; Grauslund, J.; Haffner, S.; Hamman, R. F.; Ikram, M. K.; Kayama, T.; Klein, B. E. K.; Klein, R.; Krishnaiah, S.; Mayurasakorn, K.; O'Hare, J. P.; Orchard, T. J.; Porta, M.; Rema, M.; Roy, M. S.; Sharma, T.; Shaw, J.; Taylor, H.; Tielsch, J. M.; Varma, R.; Wang, J. J.; Wang, N.; West, S.; Xu, L.; Yasuda, M.; Zhang, X.; Mitchell, P.; and Wong, T. Y. 2012. Global Prevalence and Major Risk Factors of Diabetic Retinopathy. *Diabetes Care*, 35(3): 556–564.
- Yu, S.; Ma, K.; Bi, Q.; Bian, C.; Ning, M.; He, N.; Li, Y.; Liu, H.; and Zheng, Y. 2021. MIL-VT: Multiple Instance Learning Enhanced Vision Transformer for Fundus Image Classification. In de Bruijne, M.; Cattin, P. C.; Cotin, S.; Padoy, N.; Speidel, S.; Zheng, Y.; and Essert, C., eds., *Medical Image Computing and Computer Assisted Intervention – MICCAI 2021*, 45–54. Cham: Springer International Publishing. ISBN 978-3-030-87237-3.
- Zeng, X.; Chen, H.; Luo, Y.; and Ye, W. B. 2019. Automated Diabetic Retinopathy Detection Based on Binocular Siamese-Like Convolutional Neural Network. *IEEE Access*, 7: 30744–30753.
- Zhou, G.; Pan, H.; Staudinger, S.; Wang, Y.; Liu, J.; Fleifil, S.; Jin, C.; Valikodath, N.; McNabb, R. P.; Kuo, A. N.; and Draelos, M. 2025. Mobile Robotic Optical Coherence Tomography System for Ophthalmic Imaging in Clinical Environments. In *2025 International Symposium on Medical Robotics (ISMR)*, 1–7.